NUMERICAL INVESTIGATION OF THE INFLUENCE OF CIRCULAR FILLINGS ON THE FAILURE MECHANISM IN SAMPLES CONTAINING NONPERSISTENT JOINTS UNDER SHEAR LOADING CONDITIONS

Y. Zhou,[a] J. W. Fu,[b] D. C. Wang,[b] H. Haeri,[b,1]   UDC 539.3
L. J. Sun,[c] and C. L. Guo[c]

In the current research, the influence of filling on the failure mechanism of nonpersistent joints under applied shear stress has been scrutinized using particle flow code (PFC2D). Additionally, the effects of nonpersistent joints on tunnel stability in jointed samples have been investigated. First, to reproduce the concrete specimen, PF2D was calibrated. The modeled samples with dimensions of 100×100 mm were numerically solved. The notch lengths were 15, 10, and 5 mm. The circular filling was situated in the middle part of the model, and the filling diameter was 30 mm. Gypsum materials have been employed to study the filling of modeled samples. The flat joint model was used for calibration. The tensile strengths of the concrete and gypsum samples were 3.4 and 1.4 MPa, respectively. Finally, shear tests were carried out on nine models. A shear load of 0.001 mm/sec was applied until the model's failure occurred. The results indicated that for fixed notch lengths and under normal loading conditions, shear cracks were induced in the filling layer. The tensile cracks were initiated from the original crack (joint) tips and extended within the model until coalescence with other joints and extended toward the model's boundaries. The maximum shear displacements accompanied by the shear strengths of the models increased with decreasing joint filling for the fixed notch lengths.

Keywords: shear strength, bridge area, filling, PFC2D.

Introduction. The nonpersistence joints dominate most rock masses where the engineering structures are based and excavated through them and have affected tunnel stability. The bridge areas (the distance between two joints) are the intact rock portions left between the joints in large rock masses, and the nonpersistency of joints is due to these versatile phenomena. Therefore, due to the pivotal effect of joint size (persistence) on the rock mass strength, it should be evaluated precisely during field surveys [1]. A combined shear plane could generally form during the model's failure due to the interactions of nonpersistent joints in the sample [2, 3]. In the damage zones of natural faults, nonechelon joints are the main fractures that exist in parallel fractures [4]. Several shear planes and failure zones may pass through bridge areas (the distance between two joints) in a large rock mass due to vast natural geometries and loading environments. These circumstances substantially affect the shear behavior of the fault planes within a rock mass [5, 6]. In the literature, several numerical and experimental studies have considered the mechanism of shear failures in rock specimens due to the roughness of persistent joint planes based on many circumstances [7–15]. Nevertheless, few researchers have investigated the mechanism of shear failure in rock masses, considering the effects of rock bridges and nonpersistent joints. In some previous experimental research, the embedded joints were modeled by edge notches, and the samples included exact joint configurations with different parameters [15]. Therefore, rock-like and artificial

---

    [a]Zhengzhou Metro Group Co. LTD, Zhengzhou, China. [b]School of Civil Engineering and Transportation, North China University of Water Resources and Electric Power, Zhengzhou, China ([1]haerihadi@gmail.com). [c]China Railway 14th Bureau Group Tunnel Engineering Co. LTD, Jinan, China. Translated from Problemy Mitsnosti, No. 5, p. 123, September – October, 2022. Original article submitted September 17, 2021.

materials were used to model the natural rock masses. However, mechanical characteristics such as internal friction angles and inherent shear strength and those of joints such as friction, infilling, and joint cohesion in rocks have been studied considering various loading circumstances and different geometries of individual joints and joint sets within a rock mass [5, 16–22]. On the other hand, several numerical methods have been applied to model the failure behavior of rock masses, considering the effects of nonpersistent joints and bridge areas on tunnel stability. In this work, the influence of filling on the failure mechanism of nonpersistent joints under applied shear stress was scrutinized using the code PFC2D. In the first section, the determination of micro parameters is described. Then, shear test simulation on the nonpersistent notch is introduced. The final section describes the results of the numerical simulation.

1. PFC Software. The Itasca consulting group implemented the discrete element method in the code PFC2D to solve many geo-mechanical problems in various engineering fields [23]. In this approach, the rock samples are assumed to be circular discs in contact with one another to produce the material models in the form of particle assemblies. These discs are of finite thicknesses and linked to one another by frictional bonds and cohesive properties related to their associated geomaterials [23]. The basic linear elastic models describe the displacements and forces at the contact points of the disc particles in the assembly, considering the boundary conditions and geometries of the geomaterial samples. During the loading process, tensile cracks are generated in the modeled assembly when the tensile strength of the bonds is exceeded. Additionally, shear cracks may be produced when the shear stresses surpass the shear strength of the bonds in the geomaterial assembly. The rotation of the discs may also cause anti-plane shearing in the particle assembly and produce shear cracks in the modeled sample. However, tensile failure at the contact points is dominant (Fig. 1). After its occurrence, the shear strength at the contact surfaces declines to that of the residual shear strength of the geomaterials, and shear cracks are then produced in the assembly (Fig. 2) [24, 25].
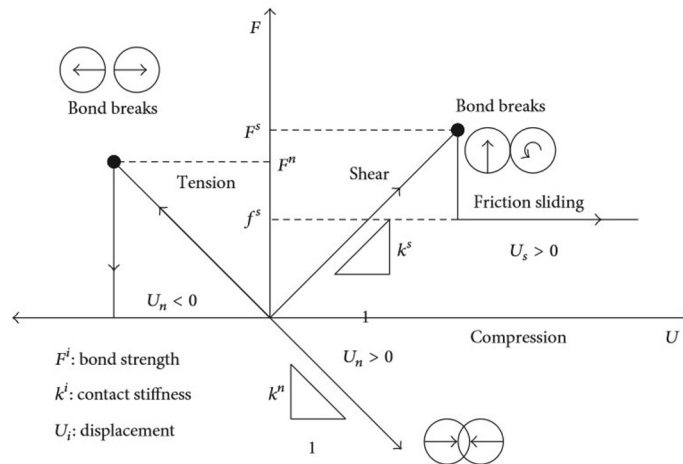

Fig. 1. Illustration of the bond yield process.

2. PFC Models for Rock Bridge and Filling Material Simulations.

2.1. Adjustment of Microparameters of Geomaterials. Indirect Brazilian tensile strength and unconfined compressive strength tests were performed on concrete specimens and gypsum as the main filling material to calibrate the PFC models in this research [16, 17]. The standard calibration algorithm proposed by Potyondy and Cundall [24] and the microparameters given by Ghazvinian et al. [16] were adopted to calibrate the geomaterial specimens and provide the calibrated particle assemblies for PFC models with rock bridges. The numerical results for the compression tests modeled in PFC are given in Fig. 2a. The tensile and shear cracks are represented by the black and red lines, respectively, in this figure. The tensile cracks are induced in the model and propagate as occurred in the valid

experimental tests. The experimental Brazilian test results and their corresponding numerical modeling results are indicated in Fig. 2b and 2c, respectively. Excellent conformity exists between the numerically simulated test results and experimental tests.
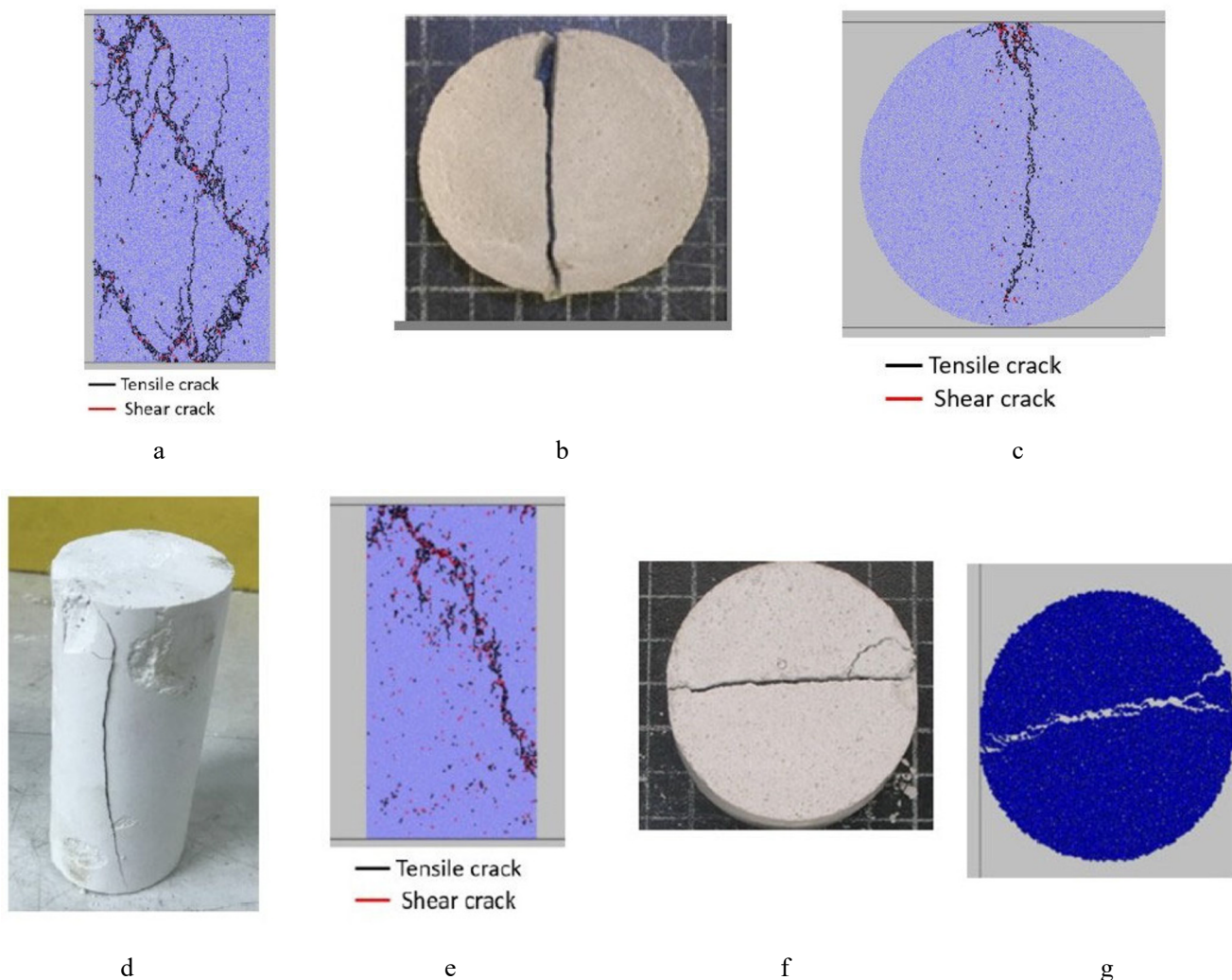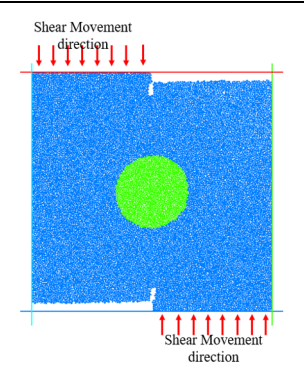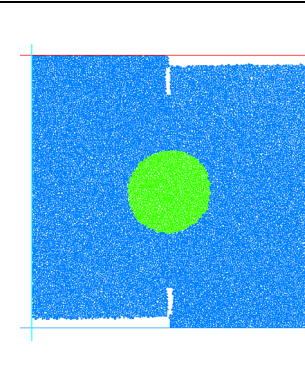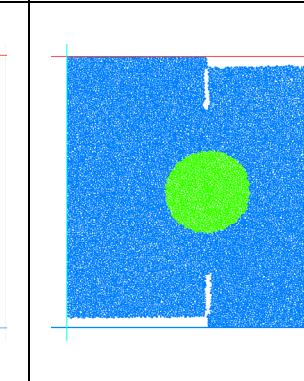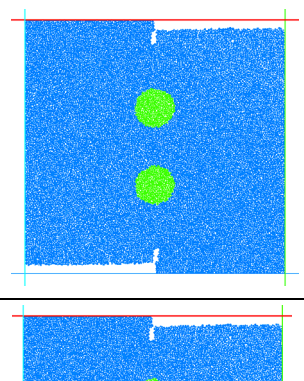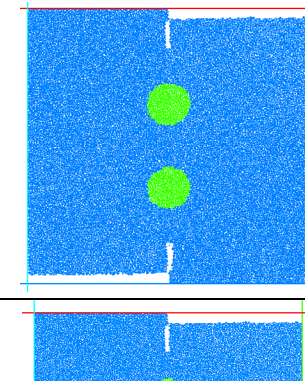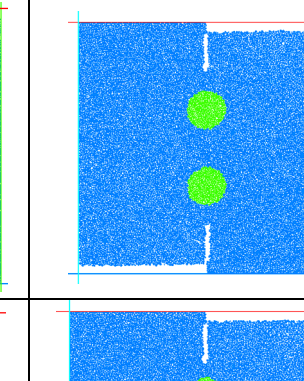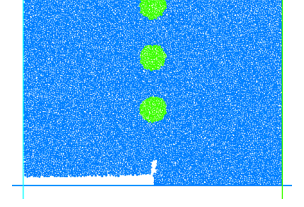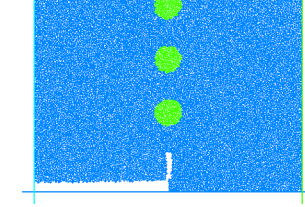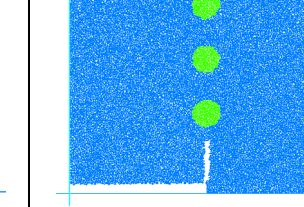

Fig. 2. Simulation of concrete (a–c) and gypsum (f–g) compression behavior: (a) numerical test; (b) experimental Brazilian disk test; (c) numerical simulation of case (b); (d) experimental compression test; (e) numerical simulation of compression test; (f) experimental Brazilian disk test on gypsum; (g) numerical simulation of case (f).

The mechanical specifications extracted from the numerical simulation are compared with the experimental results and are tabulated in Table 1. The results indicate acceptable conformity between the results of the experiments and simulations. The uniaxial and Brazilian tests were simulated numerically to calibrate the filling material. The experimental tests of uniaxial compression on the cylindrical specimens of geomaterials are given in Fig. 2d. On the other hand, Fig. 2e demonstrates the results of the numerically simulated models by PFC2D. The results for Brazilian tests and their corresponding numerically modeled discs are given in Fig. 2f and 2g, respectively. It is concluded that all numerically modeled results conform to their experimental tests performed in the laboratory. Finally, a complete comparison between the simulation and experimental results is accomplished and tabulated in Table 1, which indicates excellent agreement between these two sets of results. Based on these calibrations, the concrete and gypsum specimens were chosen for rock bridge materials and filling material, respectively.

TABLE 1. Mechanical Properties of the Materials under Study

Concrete (rock bridge)	Numerical output	Experimental result
Uniaxial compressive strength (MPa)	37.4	37.2
Young modulus (GPa)	19.3	19.1
Tensile strength (MPa)	3.4	3.3
Gypsum (filling)	Numerical output	Experimental result
Uniaxial compressive strength (MPa)	7.4	7.2
Young modulus (GPa)	9.3	9.1
Tensile strength (MPa)	1.4	1.3

TABLE 2. Numerical Models with Different Filling and Notch Configurations

2.2. Model Preparation Using Particle Flow Code. The appropriate rectangular models are prepared for PFC2D. These models properly simulate the concrete specimens using the calibrated microparameters, and shear tests have been simulated after the calibration of PFC2D (Table 2). The dimensions of the PFC specimen were 10×10 cm. To prepare for the shear test condition, two horizontal particle bands have been omitted from the top and bottom of the modeled assembly. Then, to create the nonpersistent joint, two narrow vertical bands of particles are removed from the model (Table 2). The circle space, filled with gypsum filling material, was removed from the middle part of the model.

The filling diameter was 30 mm, and in a constant filling diameter, the filling number was different, i.e., 1, 2, and 3 (Table 2). These models are loaded under shear loading, and the shear force was obtained from the recorded reaction forces on the upper wall of the model. The normal pressure was 3 MPa ($\sigma_c/3$).

3. Numerical Simulation Results.

3.1. Failure Pattern in the Numerical Model. Figures 3–5 illustrate the failure pattern of filling and the rock bridge for various notch lengths and filling numbers. However, in these figures, the induced tensile and shear cracks are indicated by red and black lines, respectively.

3.1.1. One Filling. When the notch length was 15 mm (Fig. 3a), shear cracks were initiated within the gypsum filling under normal loading. By initiating the shear displacement, both the shear cracks and tensile cracks expanded in the rock bridges and brought the model to failure. Shear cracks were initiated in the final stage of shear loading near the peak shear stress, and the number of tensile cracks exceeded the number of shear cracks. These failure processes occurred for another notch length (Fig. 3b and 3c).
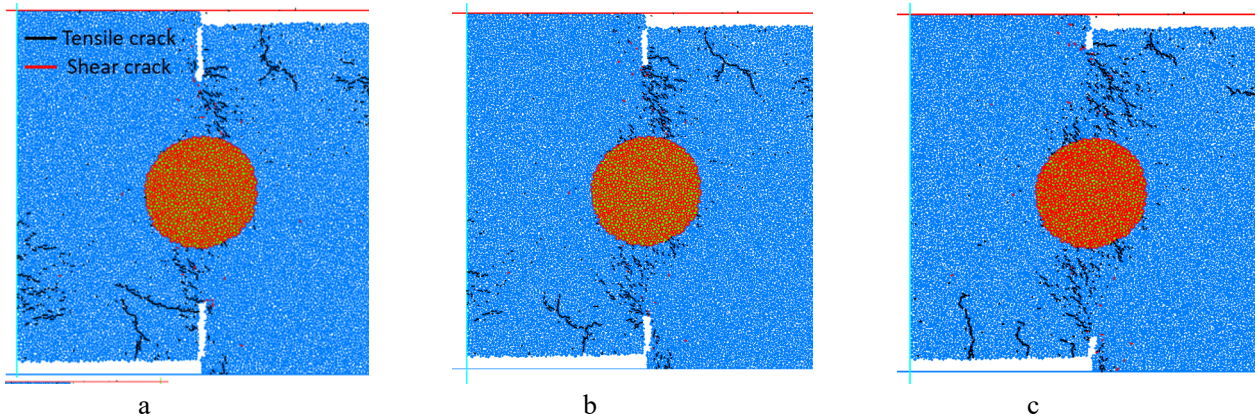

| a | b | c |

Fig. 3. Failure pattern of filling and rock bridge with notch length of 15 mm (a), 10 mm (b), and 5 cm (c); one filling.

3.1.2. Two Fillings. When the notch length was 15 mm (Fig. 4a), shear cracks were initiated within the gypsum filling under normal loading. By initiation of the shear displacement, both the shear cracks and tensile cracks expanded in bridge areas and brought the model to failure. It should be noted that some tensile fractures were expanded from the model edge due to normal loading influence. These failure processes occurred for other notch lengths (Fig. 4b and 4c).
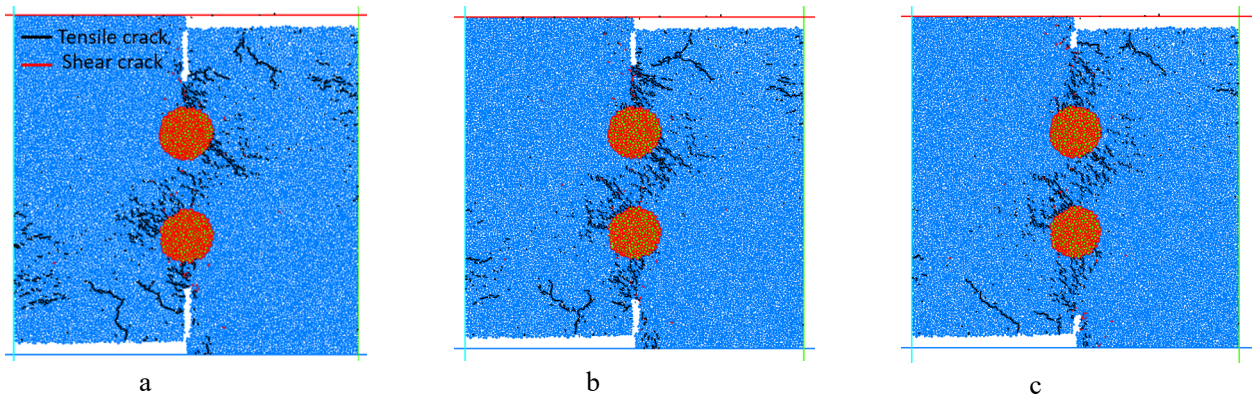

| a | b | c |

Fig. 4. Failure pattern of filling and rock bridge with notch length of 15 mm (a), 10 mm (b), and 5 cm (c); two fillings.

3.1.3. Three Fillings. When the notch length was 15 mm (Fig. 5a), shear cracks were initiated within the gypsum filling under normal loading. By initiation of the shear displacement, both the shear cracks and tensile cracks expanded in bridge areas and brought the model to failure. Shear cracks were initiated in the final stage of shear loading near the peak shear stress. Note that some tensile fractures were expanded from the model edge due to the normal loading effect. These failure processes occurred for other notch lengths (Fig. 5b and 5c).
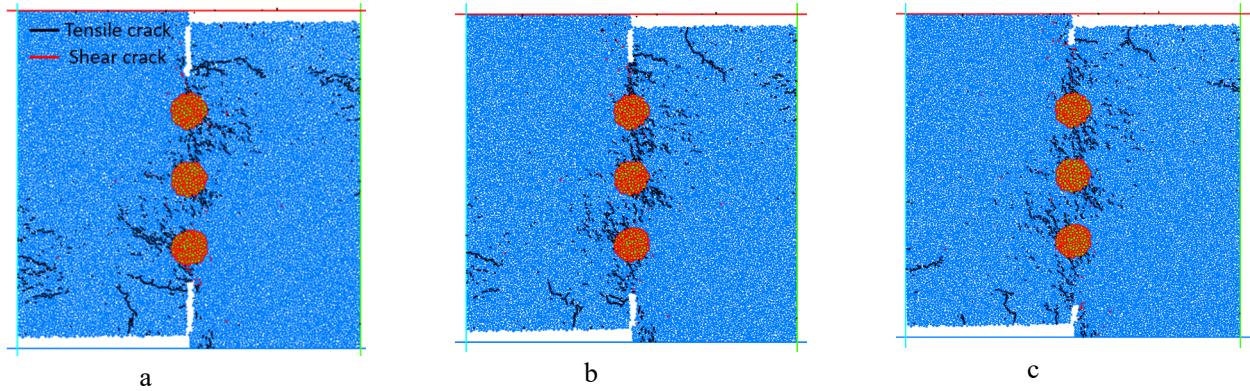

a   b   c

Fig. 5. Failure pattern of filling and rock bridge with notch length of 15 mm (a), 10 mm (b),

and 5 cm (c); three fillings.

3.2. Crack Growth Patterns Shown in the Ross Diagrams. Figures 6–8 illustrate the related Ross diagrams of the crack growth patterns considering all configurations of the notched model samples. In these analyses, the microcrack inclination angles changed from 10 to 170 degrees. By decreasing the notch length, the number of microcracks with angles of 10 and 170 degrees declined.
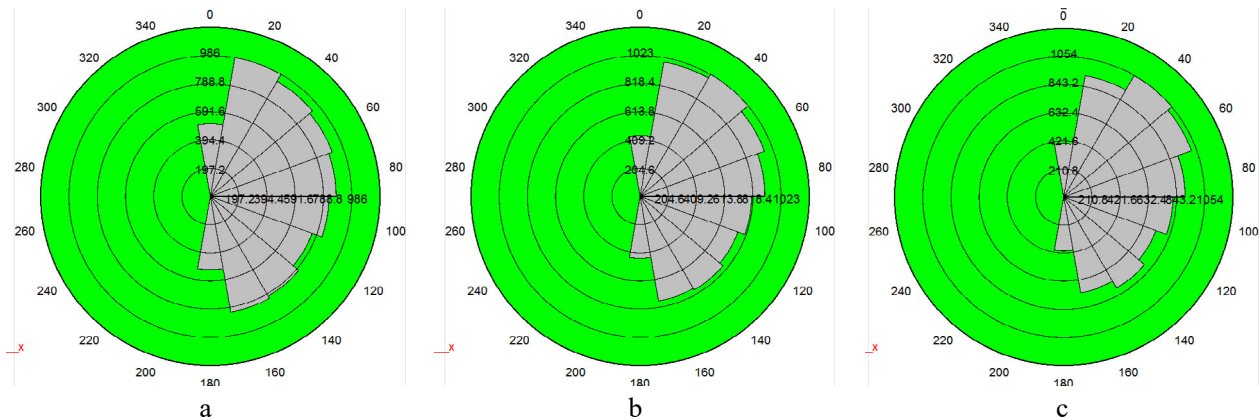

a   b   c

Fig. 6. Crack growth patterns using a Ross diagram for notch lengths of 15 mm (a), 10 mm (b),
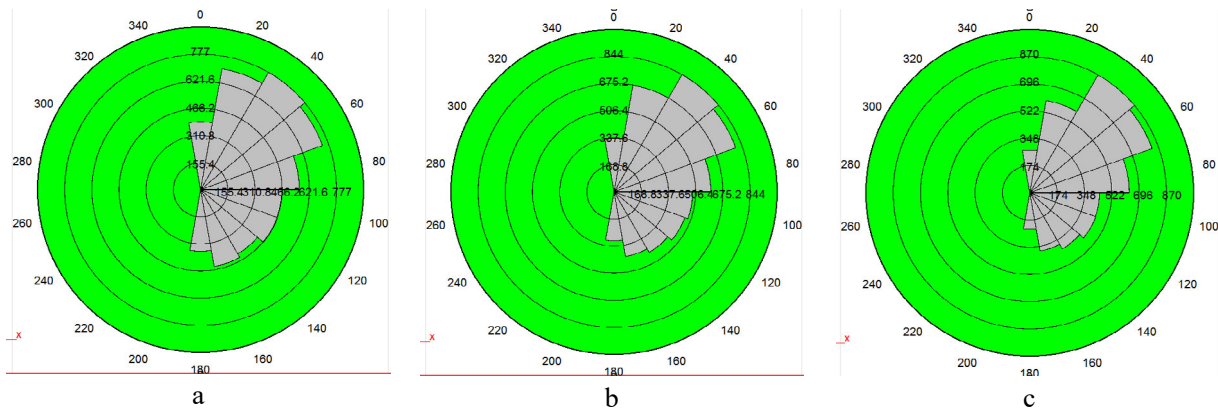
and 5 cm (c); one filling.

Fig. 7. Crack growth patterns using a Ross diagram for notch lengths of 15 mm (a), 10 mm (b), and 5 cm (c); two fillings.
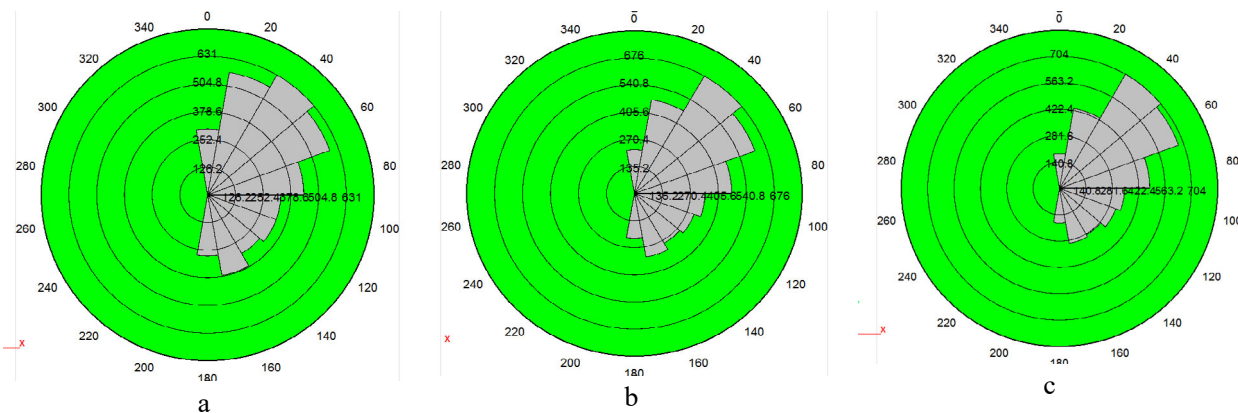

Fig. 8. Crack growth patterns using a Ross diagram for notch lengths of 15 mm (a), 10 mm (b), and 5 cm (c); three fillings.

3.3. The Influence of Bridge Area Length on the Shear Strength in the Fixed Value of Filling Width.

Figure 9 illustrates the effect of notch length on the shear strength of the numerical model for different values of filling numbers. The results indicate that in the fixed value of the filling number, the shear strength declined by enhancing the notch length. Based on fracture mechanics theory, by enhancing the notch length, the stress intensity at the tip of the joint was enhanced. Moreover, in the fixed value of filling diameter, the shear strength declined by enhancing the filling number.
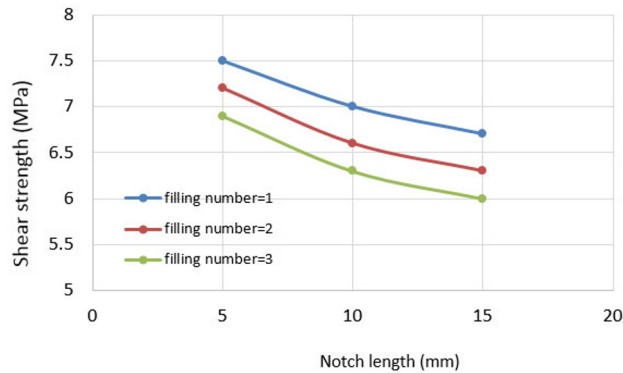

Fig. 9. Notch length on the shear strength for different filling numbers.

3.4. Effect of Bridge Area Length on the Maximum Shear Displacement at a Fixed Value of Filling Width.
Figure 10 illustrates the effect of notch length on the maximum shear displacement of the numerical sample in the fixed value of the filling number. The results indicate that in the fixed value of the filling number, by enhancing the notch length, the maximum shear displacement declined. Furthermore, in the fixed value of filling diameter, the shear displacement was reduced by enhancing the filling number.
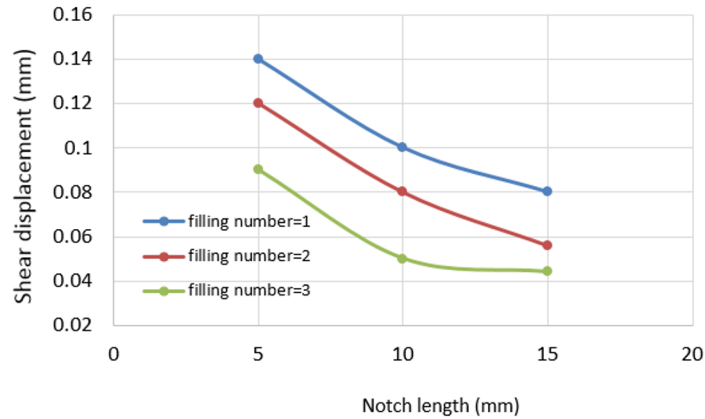

Fig. 10. Notch length effect on the maximum shear displacement for different numbers of fillings.

4. Discussion. When the notch length was 15 mm, shear cracks were initiated within the gypsum filling under normal loading. By initiating the shear displacement, both the shear cracks and tensile cracks expanded in the rock bridges and brought the model to failure. There were more tensile cracks than shear cracks, and shear cracks initiated in the final stage of shear loading near the peak shear stress. These failure processes occurred for another notch length when the filling was wide and fixed, and the shear strength was enhanced by enhancing the bridge area length. The maximum shear displacement is reduced by enhancing the notch length. Moreover, in the fixed value of filling diameter, the shear displacement declined by enhancing the filling number. These findings help researchers identify the shear behavior of soft filling. The authors intend to study the shear behavior of hard filling under various normal loadings in the future.

Conclusions. In the current research, by utilizing code PFC2D, the effects of filling and nonpersistent joints on the failure mechanism and tunnel stability under shear loading have been studied. The results indicate the following:

1. At a fixed value of the filling number, by enhancing the notch length, the shear strength declined. Based on fracture mechanics theory, by enhancing the notch length, the stress intensity at the tip of the joint is enhanced, which leads to a decrease in the shear strength. Furthermore, in the fixed value of filling diameter, the shear strength decreased as the filling number increased.

2. When the filling number is fixed, the maximum shear displacement declines by enhancing the notch length. Moreover, in the fixed value of filling diameter, the shear displacement has been reduced by enhancing the filling number.

3. In these analyses, the microcrack angles changed from 10 to 170 degrees as the notch angles and microcrack numbers changed accordingly.

REFERENCES

1. J. J. Song, "Distribution-free method for estimating size distribution and volumetric frequency of rock joints," *Int. J. Rock Mech. Min. Sci.*, **46**, 748–760 (2009).

2. Q. Deng and P. Zhang, "Research on the geometry of shear fracture zones," *J. Geophys. Res. Solid Earth*, **89**, 5699–5710 (1984).

3. P. Segall and D. D. Pollard, "Nucleation and growth of strike slip faults in granite," *J. Geophys. Res. Solid Earth* , **88**, 555–568 (1983).

4. Y. Cheng, L. N. Y. Wong, and C. Zou, "Experimental study on the formation of faults from en-echelon fractures in Carrara marble," *Eng. Geol.*, **195**, 312–326 (2015).

5. C. Gehle and H. K. Kutter, "Breakage and shear behaviour of intermittent rock joints," *Int. J. Rock Mech. Min. Sci.*, **40**, 687–700 (2003).

6. Z. Tuckey and D. Stead, "Improvements of field and remote sensing methods for mapping discontinuity persistence and intact rock bridges in rock slopes," *Eng. Geol.*, **208**, 136–153 (2016).

7. J. P. Seidel and C. M. Haberfield, "A theoretical model for rock joints subjected to constant normal stiffness direct shear," *Int. J. Rock Mech. Min. Sci.*, **39**, 539–553 (2002).

8. Y. Jiang, B. Li, and Y. Tanabashi, "Estimating the relation between surface roughness and mechanical properties of rock joints," *Int. J. Rock Mech. Min. Sci.*, **43**, 837–846 (2006).

9. Y. Ge, P. H. S.W. Kulatilake, H. Tang, and C. Xiong, "Investigation of natural rock joint roughness," *Comput. Geotech.*, **55**, 290–305 (2014).

10. Y.-K. Lee, J.-W. Park, J.-J. Song, "Model for the shear behavior of rock joints under CNL and CNS conditions," *Int. J. Rock Mech. Min. Sci.*, **70**, 252–263 (2014).

11. Y. Ge, H. Tang, M. A. M. Ez Eldin, et al., "Evolution process of natural rock joint roughness during direct shear tests," *Int. J. Geomech.*, **17**, E4016013 (2017).

12. S. H. Prassetyo, M. Gutierrez, and N. Barton, "Nonlinear shear behavior of rock joints using a linearized implementation of the Barton–Bandis model," *J. Rock Mech. Geotech. Eng.*, **9**, 671–682 (2017).

13. Q. Zhang, X. Li, B. Bai, and H. Hu, "The shear behavior of sandstone joints under different fluid and temperature conditions," *Eng. Geol.*, **257**, 105143 (2019).

14. R. Liu, S. Lou, X. Li, et al., "Anisotropic surface roughness and shear behaviors of rough-walled plaster joints under constant normal load and constant normal stiffness conditions," *J. RockMech. Geotech. Eng.*, **12**, 338–352 (2020).

15. A. Ghazvinian, M. R. Nikudel, and V. Sarfarazi, "Effect of rock bridge continuity and area on shear behavior of joints," in: Proc. of the Int. Soc. for Rock Mechanics and Rock Engineering, Lisbon, Portugal (2007).

16. A. Ghazvinian, V. Sarfarazi, W. Schubert, and M. Blumel, "A study of the failure mechanism of planar non-persistent open joints using PFC2D," *Rock Mech. Rock Eng.*, **45**, 677–693 (2012).

17. M. Jiang, J. Liu, G.B Crosta, and T. Li, "DEM Analysis of the effect of joint geometry on the shear behavior of rocks," *Comptes Rendus Mécanique*, **345**, 779–796 (2017).

18. D. Elmo, D. Donati, and D. Stead, "Challenges in the characterisation of intact rock bridges in rock slopes," *Eng. Geol.*, **245**, 81–96 (2018).

19. D. Shaunik and M. Singh, "Strength behaviour of a model rock intersected by non-persistent joint," *J. Rock Mech. Geotech. Eng.*, **11**, 1243–1255 (2019).

20. J. Shang, Z. Zhao, J. Hu, and K. Handley, "3D Particle-based DEM investigation into the shear behaviour of incipient rock joints with various geometries of rock bridges," *Rock Mech. Rock Eng.*, **51**, 3563–3584 (2018).

21. C. Romer and M. Ferentinou, "Numerical investigations of rock bridge effect on open pit slope stability," J. *Rock Mech. Geotech. Eng.*, **11**, 1184–1200 (2019).

22. M. Bahaaddini, G. Sharrock, and B. K. Hebblewhite, "Numerical investigation of the effect of joint geometrical parameters on the mechanical properties of a non-persistent jointed rock mass under uniaxial compression," *Computers and Geotechnics*, **49**, 206−225 (2013).

23. D. O. Potyondy and P. A. Cundall, "A bonded-particle model for rock," *Int. J. Rock Mech. Min. Sci.*, **41**, No. 8, 1329–1364 (2004).

24. V. Sarfarazi, A. Ghazvinian, W. Schubert, et al., "Numerical simulation of the process of fracture of echelon rock joints," *Rock Mech Rock Eng.*, **47**, No. 4, 1355–1371 (2014).